

# Spectrum of shear modes in the neutron-star crust: Estimating the nuclear-physics uncertainties

I. Tews<sup>1,\*</sup>

<sup>1</sup>*Institute for Nuclear Theory, University of Washington, Seattle, WA 98195-1550*

We construct a model of the inner crust of neutron stars using interactions from chiral effective field theory (EFT) in order to calculate its equation of state (EOS), shear properties, and the spectrum of crustal shear modes. We systematically study uncertainties associated with the nuclear physics input, the crust composition, and neutron entrainment, and estimate their impact on crustal shear properties and the shear-mode spectrum. We find that the uncertainties originate mainly in two sources: The neutron-matter EOS and neutron entrainment. We compare the spectrum of crustal shear modes to observed frequencies of quasi-periodic oscillations in the afterglow of giant gamma-ray bursts and find that all of these frequencies could be described within uncertainties, which are, however, at present too sizeable to infer neutron-star properties from observations.

## I. INTRODUCTION

Neutron stars are remarkable objects: With masses up to  $2 M_{\odot}$  [1, 2] and typical radii of the order of 12 km [3–5], densities inside neutron stars are higher than densities accessible in experiments on earth. This makes neutron stars excellent laboratories for physical theories under extreme conditions.

A large part of the available observational data on neutron stars is linked to the physics of neutron-star crusts, which can be divided into the outer and the inner crust. The outer crust consists of a lattice of neutron-rich nuclei emerged in a sea of electrons. Deeper in the neutron star, with increasing density and neutron chemical potential, the nuclei become more and more neutron-rich. At densities of  $\rho \sim 4 \cdot 10^{11} \text{g/cm}^3$ , the neutron chemical potential becomes positive and neutrons begin to drip out of the nuclei. This is where the inner crust begins. In addition to free neutrons, inhomogeneous phases of nuclear matter, the so-called nuclear pasta phases, may appear; see, e.g., Ref. [6]. At the crust-core transition density, which is roughly half of the nuclear saturation density  $\rho_0 \sim 2.7 \cdot 10^{14} \text{g/cm}^3 \sim 0.16 \text{fm}^{-3}$ , the nuclei will dissolve and a phase of uniform nuclear matter in  $\beta$  equilibrium will begin.

Understanding crustal properties is key to describe various neutron-star observations [7]. In this paper, we focus on shear properties of the neutron-star crusts: The shear modulus  $\mu$ , shear velocities  $v_S$ , and the frequency spectrum of crustal shear modes. Crustal shear modes are of particular interest for the description of quasiperiodic oscillations (QPOs) in the afterglow of giant gamma-ray bursts in magnetars [8–12]. The shear modulus describes how the neutron-star crust elastically deforms under shear stress, i.e., it describes the stiffness of the crust lattice under shear deformations. These deformations lead to the formation of shear oscillations, which travel through the crust with the shear velocity  $v_S$  and have

a frequency that depends on  $v_S$  and the crust parameters. Giant flares trigger starquakes that cause crustal shear deformations and lead to shear oscillations in the crust [13]. These shear oscillations can modulate the surface emission and then be observed as QPOs.

Because the restoring force in the crustal lattice is the Coulomb interaction, the shear modulus depends on the charge number  $Z$  of the lattice ions and their density  $n_i$ . While for the outer crust these are well understood, the composition and structure of the inner crust are not well constrained. Furthermore, additional effects in the inner crust are thought to be crucial for the correct description of crustal shear modes, like neutron superfluidity [14], entrainment of neutrons with the crust lattice [15], or the appearance of pasta phases [16, 17], but these effects are not completely understood.

This ignorance of crustal properties will also reflect in the crustal shear spectra. So far, no oscillation model, neither crustal nor global, is able to describe all observed QPO frequencies, see, e.g., Ref. [18]. On the other hand, none of these models include systematic uncertainties. In this paper, we estimate the effects of nuclear-physics uncertainties on the spectrum of crustal shear modes. These uncertainties may be sizeable and originate from various sources, e.g., the inner-crust EOS, the crust structure and composition, or neutron entrainment.

This paper is structured as follows: In Sec. II we will determine models for the inner-crust EOS within the Wigner-Seitz approximation, based on realistic interactions with systematic theoretical uncertainties. We use these EOSs in Sec. III to determine the shear modulus and the shear velocities of the neutron-star inner crust. Finally, in Secs. IV and V, we calculate the frequencies of the fundamental crustal shear oscillations as well as of the first radial overtone with nuclear-physics uncertainties with the goal of identifying the largest sources of uncertainty. We summarize and give an outlook in Sec. VI.

\* E-mail: itews@uw.edu

## II. INNER-CRUST EQUATION OF STATE

We use a Gibbs construction within the Wigner-Seitz approximation to determine an inner-crust EOS consistent with realistic models of the nuclear interactions. For the outer crust, we will use the model by Baym, Pethick, and Sutherland (BPS) of Ref. [19] with the sequence of nuclei as calculated in Ref. [20]. Since the shear spectrum is largely insensitive to the outer-crust EOS and the exact neutron drip density [18], this choice will not affect our main results.

To describe the nuclear interactions in the inner crust, we will use two different parametrizations. First, we use an empirical parametrization suggested in Ref. [4] fit to realistic interactions from chiral effective field theory (EFT) [21, 22]. Chiral EFT is a systematically improvable framework to describe low-energy hadronic interactions, and is directly connected to the symmetries of quantum chromodynamics. It naturally includes both two-body and many-body forces, which are key for the correct description of nuclei and nuclear matter, see Ref. [23] and references therein. Due to its systematics, chiral EFT allows for systematic uncertainty estimates, which enables us to investigate the effects of uncertainties in the nuclear interactions on the crustal shear spectrum. Chiral EFT has been very successfully used in calculations of nuclear matter [24–36] and nuclei [37–49], and was also used to study neutron-star properties [4, 50].

Second, we will explore the simpler parametrization suggested in Ref. [51], where the parameters were fit in Ref. [52] both to phenomenological interactions of the Argonne + Urbana/Illinois type as well as to a set of chiral EFT interactions.

### A. Inner crust from chiral EFT interactions

In the Wigner-Seitz approximation, we consider a spherical Wigner-Seitz cell of pure neutron matter, phase I, with radius  $R_W$  and volume  $V_W$ . In its center, we assume a nucleus in form of a spherical drop of asymmetric nuclear matter, phase II, with radius  $R_0$ , volume  $V_0$ , and proton number  $Z$ . The proton density is constant inside the nucleus,  $n_p^C(\mathbf{r}) = e n_p \Theta(r - R_0) = eZ/V_0 \Theta(r - R_0)$ . A relativistic electron gas is equally distributed in the Wigner-Seitz cell. The whole system is considered at  $T = 0$ .

For the two phases to be stable, the following two conditions need to be fulfilled: First, the pressure  $P(n, x) = n^2 \partial(E/A)/\partial n$  in both phases has to be equal,  $P(n, x) = P^I(n_n, 0) = P^{II}(n, x)$ , with the neutron number density in phase I,  $n_n$ , and the baryon number density  $n$  and proton fraction  $x = n_p/n$  in phase II. Second, the neutron chemical potential,  $\mu_n = \mu_p + \mu_{el}$ , has to be equal in both phases. Since the Wigner-Seitz cell is immersed in a uniform electron gas, the equilibrium conditions are not affected by the presence of electrons, and we can include their contributions later.

The neutron and proton chemical potentials  $\mu_n$  and  $\mu_p$  are given by

$$\mu_p(n, x) = n \frac{\partial(E/A)}{\partial n} + \frac{\partial(E/A)}{\partial x} (1 - x) + \frac{E}{A} + m_p, \quad (1)$$

$$\mu_n(n, x) = n \frac{\partial(E/A)}{\partial n} - \frac{\partial(E/A)}{\partial x} x + \frac{E}{A} + m_n, \quad (2)$$

with the neutron and proton masses  $m_n$  and  $m_p$ , respectively. The pressure and chemical potential can be derived easily from the energy per particle  $E/A$ , given in phase I by

$$\frac{E}{A}(n_n, 0) = \frac{E^{\text{nuc}}}{A}(n_n, 0), \quad (3)$$

and in phase II by

$$\frac{E}{A}(n, x) = \frac{E^{\text{nuc}}}{A}(n, x) + \frac{E^C}{A}(n, x) + \frac{E^S}{A}(n, x). \quad (4)$$

The term  $E^{\text{nuc}}$  takes into account the kinetic energy of the nucleons as well as the nuclear interaction energy,  $E^C$  is the Coulomb energy, and  $E^S$  the surface energy of the nuclear drop.

We first make use of the parametrization of Ref. [4], given by

$$\begin{aligned} \frac{E^{\text{nuc}}}{A}(n, x) = T_0 & \left( \frac{3}{5} \left( x^{\frac{5}{3}} + (1-x)^{\frac{5}{3}} \right) \left( \frac{2n}{n_0} \right)^{\frac{2}{3}} \right. \\ & - [(2\alpha - 4\alpha_L)x(1-x) + \alpha_L] \cdot \frac{n}{n_0} \\ & \left. + [(2\eta - 4\eta_L)x(1-x) + \eta_L] \cdot \left( \frac{n}{n_0} \right)^\gamma \right), \end{aligned} \quad (5)$$

where  $n_0$  is the nuclear saturation density,  $n_0 = 0.16 \text{ fm}^{-3}$ ,  $T_0 = (3\pi^2 n_0/2)^{2/3} \hbar^2/(2m_N)$  is the Fermi energy of symmetric nuclear matter at saturation density, and  $\gamma = 4/3$ . The parameters  $\alpha, \alpha_L, \eta$ , and  $\eta_L$  are determined from fits to the empirical saturation point,  $\frac{E^{\text{nuc}}}{A}(n_0, 0.5) = -16 \text{ MeV}$ , and  $P^{\text{nuc}}(n_0, 0.5) = 0$ , and to the neutron-matter results of Ref. [24] from chiral EFT. The full parameter range can be found in Ref. [4] and allows us to quantify the uncertainties of modern nuclear interactions.

This parametrization leads to an incompressibility parameter  $K = 236 \text{ MeV}$  and a skewness parameter  $K' = -384 \text{ MeV}$ . The symmetry energy  $S_v$  and its density dependence at saturation density,  $L$ , defined via

$$S_v(n) = \frac{1}{8} \frac{\partial^2 E}{\partial x^2} \frac{E}{A}(n, x) \Big|_{x=1/2}, \quad (6)$$

$$L = 3n_0 \frac{\partial}{\partial n} S_v(n) \Big|_{n_0}, \quad (7)$$

range from  $S_v = (29.7 - 33.2) \text{ MeV}$  and  $L = (32.5 - 57) \text{ MeV}$ , respectively. These ranges are in excellent agreement with experimental constraints, see, e.g.,

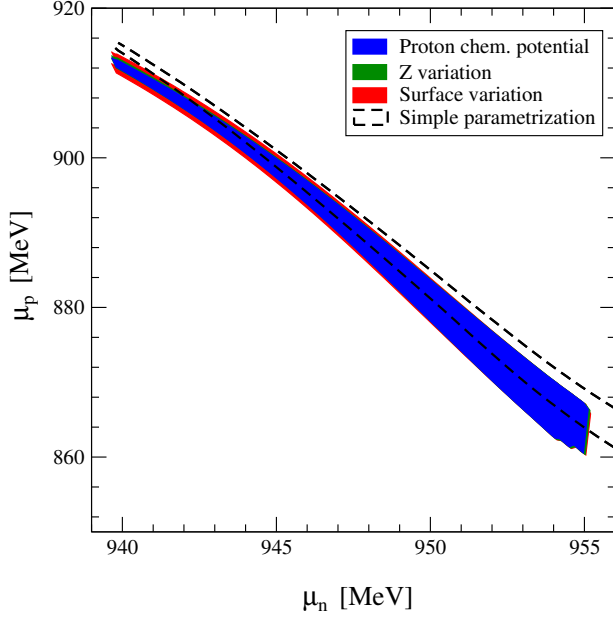


FIG. 1. Proton chemical potential as a function of the neutron chemical potential. The different bands show the uncertainties due to different sources: the variation of the surface parameters (red band), of  $Z$  (green band), and of the neutron-matter EOS (blue band). As one can see, the uncertainties are dominated by the blue band (which overlaps the red and green bands almost always completely). We also show the results obtained by using a simpler parametrization for the nuclear interaction (dashed bands), see Sec. II B.

Ref. [53], which rule out much larger values of  $L$ . Moreover, the parametrization of Eq. (5) is in remarkable agreement with explicit asymmetric-matter calculations [4, 29] and, thus, can be used with confidence to describe both neutron as well as asymmetric nuclear matter.

The Coulomb energy per particle of a nucleus with uniformly distributed protons is given by

$$\frac{E^C}{A}(n, x) = \frac{3}{5} \alpha_{\text{FS}} \hbar c \left( \frac{4\pi}{3} \right)^{\frac{1}{3}} Z^{\frac{2}{3}} n^{\frac{1}{3}} x^{\frac{4}{3}}, \quad (8)$$

with the fine structure constant  $\alpha_{\text{FS}}$ . This form is analogous to the Coulomb term in the phenomenological Bethe-Weizsaecker mass formula.

The surface energy  $E^S$  is the product of surface area and surface tension  $\sigma(x)$ ,

$$\frac{E^S}{A}(n, x) = \frac{1}{A} \sigma(x) \cdot 4\pi R_0^2 = \sigma(x) \cdot \left( \frac{36\pi x}{Zn^2} \right)^{\frac{1}{3}}. \quad (9)$$

We follow Ref. [54] and expanded the surface tension in the neutron excess  $\beta = (1 - 2x)$ ,

$$\sigma(x) = \sigma_0(1 - \sigma_\beta(1 - 2x)^2 + \dots), \quad (10)$$

where  $\sigma_\beta$  is the symmetry parameter of the surface tension. Because the surface tension measures the energy

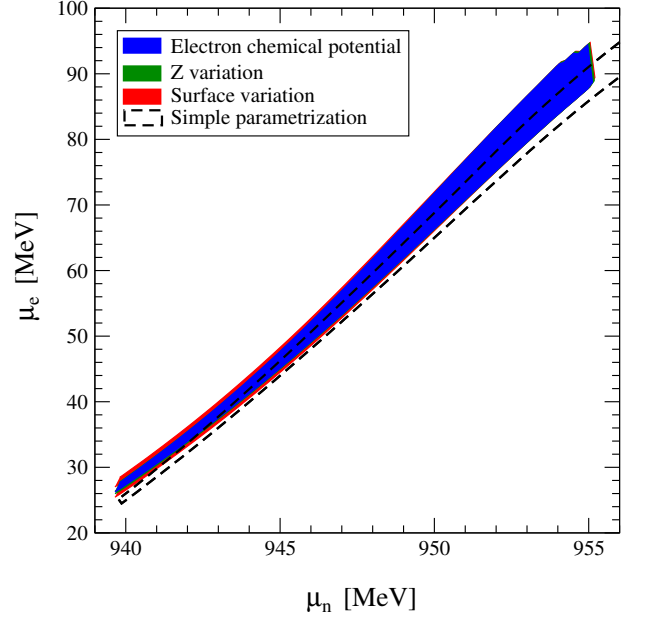


FIG. 2. Electron chemical potential as a function of the neutron chemical potential, where the bands are obtained as in Fig. 1.

needed to support the surface against the lower density in the outer phase, it has to vanish for  $x \rightarrow 0$  in the neutron-star inner crust (because in this case both phases are identical). Then, one can modify the surface tension,

$$\sigma(x) = \sigma_0 \frac{16 + b}{\frac{1}{x^3} + b + \frac{1}{(1-x)^3}}, \quad (11)$$

where  $b = 96/\sigma_\beta - 16$ . To determine the surface parameters  $\sigma_0$  and  $\sigma_\beta$ , we fit the binding energies of Eq. (4) with the surface tension as defined in Eq. (10) to the experimentally measured masses from Ref. [55]. From  $\sigma_\beta$  we determine  $b$ , and use the surface tension of Eq. (11) for the inner crust of the neutron star.

We account for uncertainties in the modelling and the fitting procedure and vary both  $\sigma_0$  and  $b$  within a 10% uncertainty. This uncertainty estimate is large enough to bring the binding energies of Eq. (4) into agreement with experimental values for all nuclei.

In addition to the nucleonic contributions to the system, we consider a free relativistic electron gas with constant electron density  $n_{el}$  in the Wigner-Seitz cell. The electron energy density is given by [7],

$$\varepsilon_{el}(n_{el}) = \frac{m_{el}^4 c^8}{8\pi^2 \hbar^3 c^3} \left( x_r (2x_r^2 + 1)(x_r^2 + 1)^{\frac{1}{2}} - \ln(x_r + (x_r^2 + 1)^{\frac{1}{2}}) \right), \quad (12)$$

with  $x_r = \hbar k_F / (m_{el} c) = (3\pi^2 n_{el})^{1/3} \hbar c / m_{el}$  and the electron mass  $m_{el} = 0.511$  MeV. For the free electron gas, this leads to an electron chemical potential of  $\mu_{el}^{\text{free}} = (\hbar^2 c^2 (3\pi^2 n_{el})^{2/3} + m_{el}^2 c^4)^{\frac{1}{2}}$  and an electron pressure,  $P_{el}(n_{el}) = n_{el} \partial \varepsilon_{el} / \partial n_{el} - \varepsilon_{el}$ .

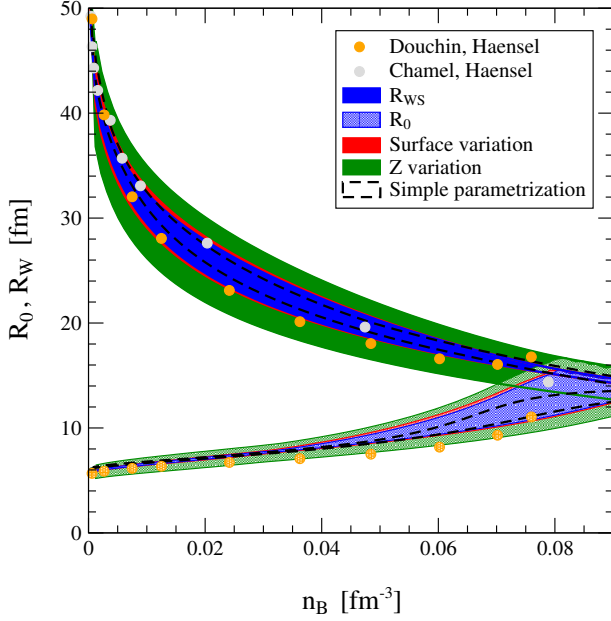


FIG. 3. Radii of the nucleus  $R_0$  (dotted, lower bands) and of the Wigner-Seitz cell  $R_W$  (filled, upper bands) as a function of baryon density. The bands are determined as in Fig. 1. We also show results by Douchin and Haensel [56] (orange points) and  $R_W$  from the calculation by Chamel and Haensel [7] (grey points).

The contribution of the electrons to the Coulomb energy is given by two terms. The first one is the lattice energy [7],

$$\varepsilon_L^C(n_{el}) = -\frac{9}{10}\alpha_{FS}\hbar c \left(\frac{4\pi}{3}\right)^{\frac{1}{3}} Z^{\frac{2}{3}} n_{el}^{\frac{4}{3}}, \quad (13)$$

and describes the electron Coulomb energy assuming point-like nuclei. The second term corrects for the finite size of the nuclei, and is given by [7],

$$\varepsilon_L^{C,corr}(n_{el}) = -\frac{1}{3}\varepsilon_L^C(n_{el})w^{\frac{2}{3}}, \quad (14)$$

where  $w = \frac{V_0}{V_W}$  is the volume fraction of the nucleus in the Wigner-Seitz cell. One can rewrite the electron Coulomb contribution in terms of  $n$  and  $x$  and include it in  $E^C$  in Eq.(8), which leads to

$$\frac{E^C}{N}(n, x) = \frac{3}{5}\alpha_{FS}\hbar c \left(\frac{4\pi}{3}\right)^{\frac{1}{3}} Z^{\frac{2}{3}} n^{\frac{1}{3}} x^{\frac{4}{3}} \times \left(1 - \frac{3}{2}w^{\frac{1}{3}} + \frac{1}{2}w\right). \quad (15)$$

To obtain the radii of the nucleus and the Wigner-Seitz cell, we first need to determine the proton number  $Z$  of the nuclei.  $Z$  can be obtained by minimizing the energy inside the Wigner Seitz cell, which is complicated as shell effects have to be considered. As a simplification, we assume that nuclei in the neutron-star crust favor configurations with closed proton shells [57] and choose  $Z = 40$ .

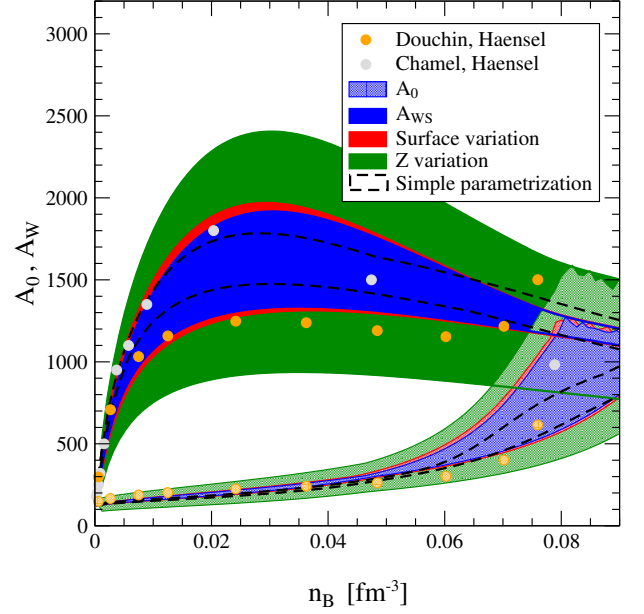


FIG. 4. Nucleon numbers of the nucleus,  $A_0$ , (dotted, lower bands) and of the Wigner-Seitz cell,  $A_W$ , (filled, upper bands) as a function of baryon density. The bands are determined as in Fig. 1. We also show results by Douchin and Haensel [56] (orange points) and  $A_W$  from the calculation by Chamel and Haensel [7] (grey points).

To account for uncertainties associated with this assumption, we vary  $Z$  in a range  $Z = 28 - 50$ , which includes the two neighbouring shell closures, and overlaps with various determinations, see Ref. [7].

For each neutron density  $n_n$ , the equilibrium conditions constrain density and proton fraction in the nuclear phase. By varying  $n_n$ , and thus, fixing the pressure and the neutron chemical potential, we can determine the composition and density of the nucleus as well as the electron chemical potential  $\mu_{el} = \mu_n - \mu_p$  and, thus, the electron density. In Figs. 1 and 2, we show the proton and electron chemical potentials  $\mu_p$  and  $\mu_e$  as functions of  $\mu_n$ . In addition to the nuclear-physics uncertainties from the neutron-matter EOS (blue band), we show the uncertainties due to the  $Z$  variation (green band) and due to variation of the surface parameters (red band).

The main uncertainty in the chemical potentials stems from the variation of the neutron-matter EOS. This is to be expected, because pressure and chemical potentials are mostly set by the bulk EOS. The  $Z$  variation has only a small effect and can be neglected even at low densities (low neutron chemical potential).  $Z$  primarily impacts the Coulomb energy, which is the smallest contribution to the energy at all densities and rapidly decreases with increasing density. The uncertainty in the surface parameters is considerable only at low densities. At higher densities,  $\sigma(x)$  (and, thus, the surface energy) decreases and its uncertainty can be neglected.

With known  $Z$  and proton density inside the nucleus, we can determine the volume of the nucleus,  $V_0 =$

$Z/n_p = Z/(nx)$ . To determine the size of the Wigner-Seitz cell,  $V_W$ , we enforce charge neutrality,  $Q = 0 = V_0 n_p - V_W n_{el}$ , and obtain  $V_W = Z/n_{el}$ . The radii  $R_0$  and  $R_W$  are plotted in Fig. 3, and the nucleon numbers  $A_0$  and  $A_W$  inside the nucleus and the Wigner-Seitz cell, respectively, are shown in Fig. 4, with similar uncertainty bands as before. It is clear that the choice of the proton number  $Z$  has the largest impact on these numbers. We compare our calculation to the results of Ref. [56] and with  $A_W$  and  $R_W$  obtained in Ref. [57] and find very good agreement.

Although we calculate all crustal properties up to the density at which the Gibbs construction breaks down, we need to determine the crust-core transition density,  $n_{cc}$ , to calculate the shear spectrum. The crust-core transition density is the density at which the Gibbs free energy of the crustal lattice becomes larger than that of uniform nuclear matter in  $\beta$  equilibrium. For our crust model we find that the transition density ranges from  $0.074 - 0.090 \text{ fm}^{-3}$ . The exact value of the crust-core transition density in principle influences the QPO frequencies calculated in Secs. IV and V, because it impacts the crust thickness  $\Delta R$ . While the fundamental mode frequencies, which mainly scale with the neutron-star radius, are almost independent of the exact transition density, the overtones depend on its exact value [18, 58]. However, since we later also vary the crust thickness in a sizeable range, any additional uncertainty in the transition density will be accounted for.

Having determined all parameters of the Wigner-Seitz cell, we can model the crust as a Coulomb lattice of Wigner-Seitz cells, with the density of nuclei,  $n_i$ , given by  $n_i = (4/3\pi R_W^3)^{-1}$ . At higher densities in the inner crust, though, matter may form nuclear pasta phases, and the Wigner-Seitz approximation will fail. We do not consider these phases in this work, which may be an additional source of uncertainty, see, e.g., Ref. [16, 17]. While the appearance of nuclear pasta phases will not affect the equilibrium conditions (pressure and neutron chemical potential at a certain  $n_n$  will be unchanged), it may affect the composition, energy density, and shear properties at higher densities in the inner crust. The elastic properties of these phases are still unknown [17] and their impact needs to be studied in future work.

### B. Inner crust from a simple parametrization

We also explore a simpler parametrization for the energy per particle and start from the four-parameter parametrization for pure neutron matter, given by [51]

$$\frac{E}{N}(n, 0) = a \left( \frac{n}{n_0} \right)^\alpha + b \left( \frac{n}{n_0} \right)^\beta, \quad (16)$$

where the parameters  $a$  and  $\alpha$  describe the low-density equation of state, while the parameters  $b$  and  $\beta$  determine the higher-density part of the EOS. We consider the parameter range given in Ref. [52], which includes fits of

these four parameters both to phenomenological interactions of the Argonne and Urbana/Illinois type as well as to selected chiral neutron matter EOS. This simple parametrization leads to a similar neutron-matter EOS compared to the empirical parametrization used before.

To describe the energy in the nuclear cluster, we expand the energy per particle for asymmetric matter around symmetric nuclear matter,

$$\begin{aligned} \frac{E}{A}(n, x) &= \frac{E}{A}(n, x=0.5) + S_v(n)(1-2x)^2 + \dots \quad (17) \\ &= -16 \text{ MeV} + \frac{1}{2} \frac{\partial^2 E}{\partial n^2} (n - n_0)^2 \\ &\quad + \frac{1}{6} \frac{\partial^3 E}{\partial n^3} (n - n_0)^3 + \dots \\ &\quad + S_v(n)(1-2x)^2 + \dots, \end{aligned}$$

where we have expanded around the saturation point. We choose the incompressibility and skewness parameters

$$\begin{aligned} K &= 9n_0^2 \frac{\partial^2 E}{\partial n^2} = 236 \text{ MeV}, \quad (18) \\ K' &= 27n_0^3 \frac{\partial^3 E}{\partial n^3} = -384 \text{ MeV}, \end{aligned}$$

consistent with the values for the previous parametrization, and approximate the symmetry energy as  $S_v(n) = \frac{E}{N}(n, 0) - \frac{E}{N}(n, x=0.5)$ . For the Coulomb energy, we use the same form as before. For the simple model, to further reduce the number of parameters, we choose the surface energy to be  $E^S/A = 2E^C/A$  [59].

The results for this simpler model are shown in each plot as a black-dashed band. For the proton chemical potentials in Fig. 1 (electron chemical potentials in Fig. 2), the results for the simple parametrization lie at the upper (lower) boundary of the results for the empirical parametrization. At low densities, the two parametrizations start to diverge, due to the simplified modeling of the surface energy. At higher densities, the simple model leads to higher (lower) proton (electron) chemical potentials due to the inclusion of fits to the Argonne+Urbana interactions, which give higher neutron-matter pressure than chiral models.

These effects are reflected in the radii and nucleon numbers in Figs. 4 and 3. A higher proton chemical potential for the same neutron chemical potential leads to a higher proton density in the nucleus. Thus, for proton chemical potentials at the upper boundary of the empirical parametrization (and a constant  $Z$ ) one would expect radii and nucleon numbers at the lower boundary. Similarly, for slightly lower electron chemical potentials one would expect slightly larger radii and nucleon numbers inside the Wigner-Seitz cell.

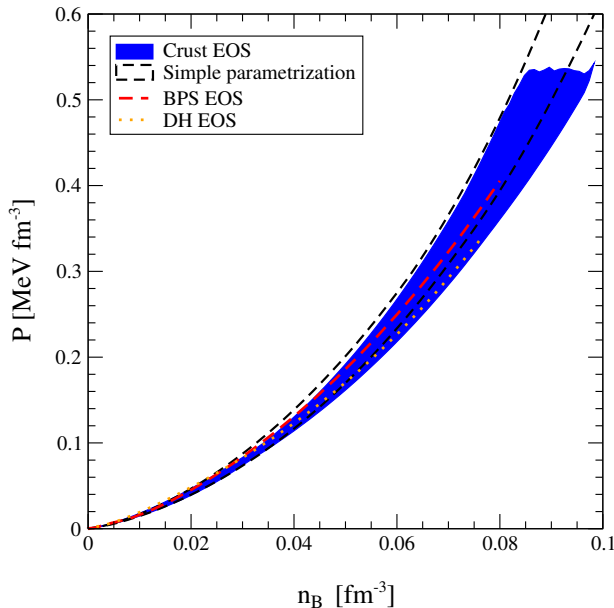


FIG. 5. Inner-crust EOS (pressure as a function of baryon density) for the inner-crust model of this work. The uncertainty band for  $P(n_B)$  solely originates in the uncertainty of the neutron-matter EOS. We also show the BPS EOS [19] and the EOS by Douchin and Haensel [56].

### C. Equation of State

As described in Sec. II A, for every input neutron density  $n_n$  in the neutron-matter phase we can determine the energy density in the Wigner-Seitz cell,

$$\varepsilon_W = w \cdot n \frac{E}{A}(n, x) + (1 - w) \cdot n_n \frac{E}{A}(n_n, 0) + \varepsilon_{el}(n_{el}), \quad (19)$$

as well as the baryon density  $n_B = w \cdot n + (1 - w) \cdot n_n$ , and the total pressure  $P = P_I + P_{el} = P_{II} + P_{el}$ . We, thus, can obtain the EOS of the inner crust,  $P = P(\varepsilon)$  or  $P = P(n_B)$ , with theoretical uncertainties. The inner-crust EOS is plotted in Fig. 5 and agrees well with the BPS EOSs [19] and the EOS by Douchin and Haensel [56].

The only source of uncertainty for the inner-crust EOS is the neutron-matter EOS. This is intuitive because for a given input density in the neutron-matter phase,  $n_n$ , the pressure is set independently of  $Z$  or the surface parameters. At the same time, the baryon density is determined primarily by the neutron-matter density: Variation of the surface and Coulomb energies, by variation of  $Z$  and the surface parameters, is only relevant at low densities, where the neutron-matter phase dominates the volume of the Wigner-Seitz cell. The main effect of the  $Z$  variation is a change of the volumes of the Wigner-Seitz cell and the nucleus by the same factor and, thus, these volume changes do not affect the energy or baryon density.

When calculating the equation of state with the simple parametrization, we find very good agreement with the

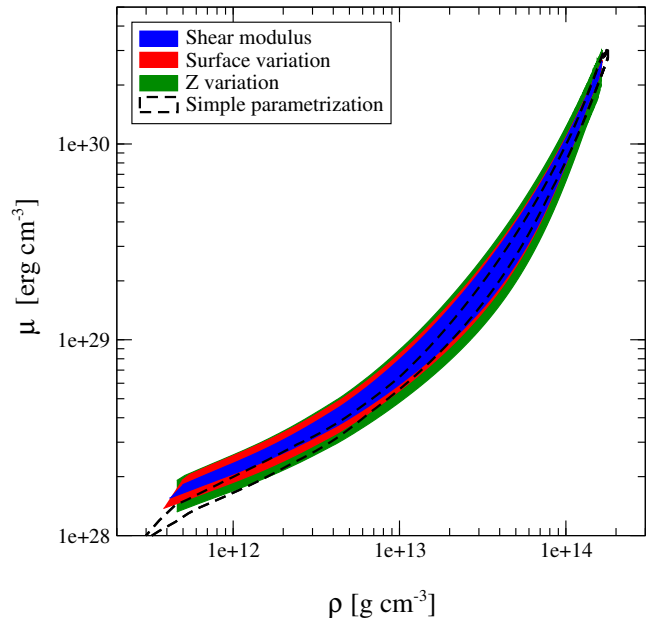


FIG. 6. Shear modulus as a function of mass density, where the uncertainty bands are obtained as in Fig. 1.

empirical parametrization, see Fig. 5. This is expected, as both models describe the neutron-matter EOS similarly as well as the empirical saturation point.

### III. SHEAR MODULUS AND SHEAR VELOCITIES

The shear modulus for a body-centered cubic Coulomb lattice in the neutron-star crust is given by Ref. [60]

$$\mu = \frac{0.1194}{1 + 0.595(\Gamma_0/\Gamma)^2} \frac{n_i(Ze)^2}{a}. \quad (20)$$

Here,  $n_i$  is the density of nuclei, and  $a = (3/(4\pi n_i))^{1/3}$ . The parameter  $\Gamma = (Ze)^2/ak_B T$  with temperature  $T$  and the Boltzmann constant  $k_B$  is the ratio of Coulomb and thermal energy. The upper boundary of the crust is defined as  $\Gamma_0 = 173$  [61]. Assuming  $T = 0$  and including electron screening effects [62],  $\mu$  is given by

$$\mu = 0.1194 \left(1 - 0.010Z^{2/3}\right) \frac{n_i(Ze)^2}{a}. \quad (21)$$

We use this form for the shear modulus throughout the whole crust and neglect possible effects of nuclear pasta phases on  $\mu$ , which could be sizeable [16, 17].

Using the properties of the Wigner-Seitz cell,  $n_i = 1/V_W$ , and  $a = R_W$ , we obtain the shear modulus in the neutron-star inner crust and show our results in Fig. 6. Since the shear modulus is purely geometrical and only depends on  $R_W$ , the uncertainties in the EOS and in  $Z$  are dominant. Using the simple parametrization, we find very good agreement at higher densities. For lower densities, at the top of the inner crust, both parametrizations

start do disagree, which is a direct consequence of the higher  $R_W$ , see Fig. 3.

The shear velocities in the crust follow from the shear modulus,  $v_S = (\mu/\rho_c)^{\frac{1}{2}}$ , with  $\rho_c$  being the dynamical mass density (which is the mass density of nucleons moving with the lattice). When neglecting the effects of neutron superfluidity, the dynamical mass density equals the total mass density,  $\rho_c = \rho$  [18]. Neutron superfluidity, however, plays an important role in neutron star modelling [14] because free superfluid neutrons typically do not add to the dynamical mass density. They are unlocked from the movement of the lattice and do not affect the shear properties of the crust. This effect can reduce  $\rho_c$  considerably compared to  $\rho$  [14], leading to larger shear velocities.

In reality, the unbound superfluid neutrons, however, still interact with the lattice due to Bragg scattering, which can effectively lock a considerable portion of them in the lattice (entrained neutrons). Reference [15] found that up to 90% of unbound neutrons could be entrained with the lattice, and, thus, only a small fraction of neutrons would be effectively free (conduction neutrons). The density of entrained neutrons,  $n_n^{ent}$ , the density of all unbound neutrons,  $n_n^{ub}$ , and the density of conduction neutrons,  $n_n^c$ , are related,

$$n_n^{ent} = n_n^{ub} - n_n^c = n_n^{ub} \left(1 - \frac{n_n^c}{n_n^{ub}}\right) = n_n^{ub} \cdot R_e, \quad (22)$$

where we define  $R_e$  as the fraction unbound neutrons that are entrained. We use the density-dependent values for entrainment from Ref. [15], which were determined using Skyrme potentials. Because these values are model dependent and not consistently derived for the chiral interactions we use throughout this work, we will associate large uncertainties with them. We will vary  $R_e$  starting from no entrainment at all,  $n_n^c/n_n^{ub} = 1, R_e = 0$ , up to full entrainment of all neutrons,  $n_n^c/n_n^{ub} = 0, R_e = 1$ . The latter case is equivalent to setting  $\rho_c = \rho$  as in Ref. [18]. While this range of variation appears to be large, the values for  $R_e$  calculated in Ref. [15] themselves vary between 0.3 and 0.9 in the density range relevant for the neutron-star inner crust. Furthermore, Ref. [62] suggested a sizeable correction factor of  $\approx 0.4$  to these values.

The variation in  $R_e$  leads to a variation of shear velocities, with the minimum obtained for  $R_e = 1$  and the maximum for  $R_e = 0$ . Please note that the shear modulus defined in Eq. (21) is purely geometrical and, thus, does not depend on entrainment.

In Fig. 7, we show the shear velocities for the values of  $R_e$  from Ref. [15] (blue band). In addition to the uncertainty bands from  $Z$  variation (green band) and variation of the surface parameters (red band), we show the variation with  $R_e$  (light-red band) and present a combined uncertainty band (grey band). We find that the variation of the entrainment parameter has the major impact on the shear velocities: They vary within a factor of two in the density regime of interest when varying  $R_e = 0 - 1$ .

Entrainment, thus, will also have a large impact on the shear spectra, which we discuss in the next sections.

For the simple parametrization and  $R_e$  values from Ref. [15], we find good agreement of both parametrizations, which was expected based on the shear moduli. We also compare our results to the calculation of Ref. [18] (turquoise band), which was obtained using  $R_e = 1$ . The shear properties of the crust are sensitive to the symmetry energy,  $S_v$ , and its density dependence parameter,  $L$ . In particular, the shear velocities are anticorrelated with the  $L$  parameter. Because the chiral interactions have smaller  $L$  values compared to some of the Skyrme models used in Ref. [18], the shear velocities for chiral interactions lie at the upper boundary of the band in Ref. [18]. Considering this, both results are in very good agreement.

#### IV. FREQUENCIES OF THE FUNDAMENTAL CRUSTAL SHEAR MODE

Magnetars may provide a possibility of obtaining neutron-star shear properties by investigating giant gamma-ray bursts. These bursts are triggered when the very strong magnetic fields of the magnetars decay over time and create unstable field-line configurations. Since the field lines are pinned to the magnetar's crust, unstable configurations may exert stress on the crust, which, at a certain point, ruptures and allows the magnetic field to reconfigure [63]. While the crust rupturing produces neutron starquakes, the field-line reconfigurations create currents which dissipate and produce giant gamma-ray bursts [13].

At least three such giant bursts have been detected so far. In their afterglow, in addition to the modulation associated with the magnetar's rotation, several quasi-periodic oscillations (QPOs) in the frequency range from 18-1800 Hz were observed [8–12]. These oscillations have been interpreted as torsional shear modes of the crust [13]. Crustal shear modes have lower excitation energies compared to other vibrational modes and their excitation is plausible considering typical energy releases in giant flares [63, 65]. Furthermore, models of torsional shear modes are in qualitative agreement with many of the observed QPO frequencies and their scaling behavior.

If this interpretation were correct, QPOs could be used to infer crustal shear properties as well as to put constraints on the mass-radius relation of neutron stars. The latter is possible because different oscillation modes have different dependencies on neutron star radius, crust thickness, and mass [66]. A description of QPOs solely from crustal properties makes use of the free-slip boundary condition, meaning that crust and core can be treated independently. Because the strong magnetic fields in the magnetars couple crust and core, this approximation seems to be inaccurate in general [67], and QPOs are most likely global oscillation modes.

Initial studies of global magnetar oscillations [68, 69]



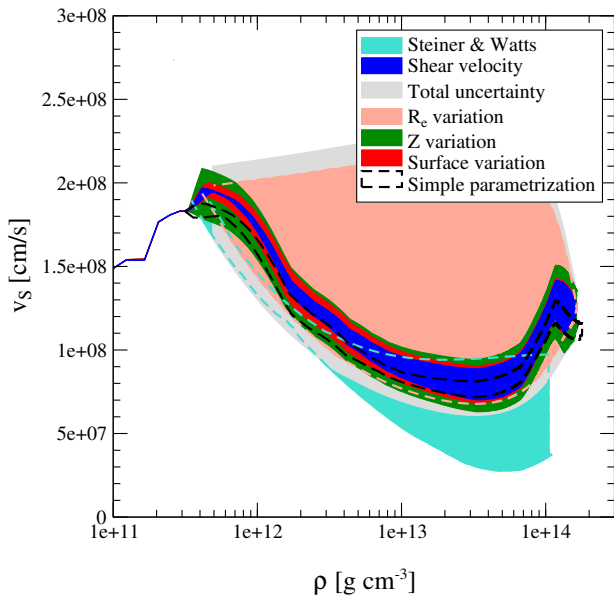


FIG. 7. Shear velocities as a function of density. In addition to the uncertainty bands from Fig. 1, we show the uncertainty in the entrainment parameter  $R_e$  (light-red band) as well as the combined total uncertainty (grey band). We compare our results with the velocity band from Ref. [18], which used various Skyrme interactions as input.

found that all crustal modes will couple with and transfer energy to the neutron-star core on a very short time scale, creating Alfvén continua. More recent studies [70, 71] found that the appearing spectrum is very rich. There will appear continua of global oscillation modes with strong signals at their endpoints. Moreover, the star will permit discrete core Alfvén modes, which are possible probes of the neutron-star core. Lastly, discrete strong crust-dominated modes will appear, which can be very close to the pure crustal modes. If these crust-dominated modes lie within the continua, they will be absorbed and disappear from the spectrum. If these modes, instead, lie in the gaps between the continua, they will be very strong. These effects complicate the correct identification of observed QPO frequencies in terms of these different oscillation modes, which is a challenging and open problem.

Assuming that at least some QPO frequencies can be described by pure crustal oscillation modes (which are close to global crust-dominated shear modes), the fundamental frequency is found to be comparable in size to the lowest observed QPO frequencies: 18, 26, and 29 Hz for the hyperflare SGR 1806-20 [11], and 28 Hz for SGR 1900+14 [9]. For example, in Ref. [18], the calculated fundamental shear mode frequencies ranged from 7 – 22 Hz and were compatible with the 18 Hz QPO. In Ref. [58], the fundamental shear mode was matched both with the 18 Hz QPO or the 28 Hz QPO, based on the employed EOS model.

In this section, we calculate the frequency of the fun-

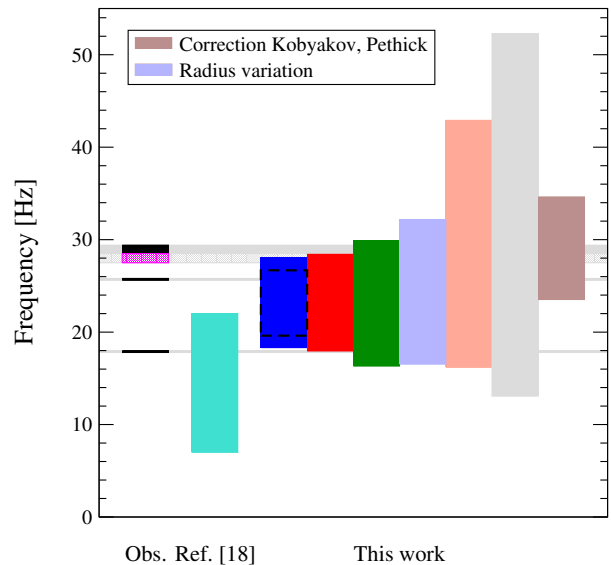


FIG. 8. Frequencies of the fundamental ( $n = 0, l = 2$ ) shear mode for the shear velocities of Fig. 7. All bands include a variation of the total neutron-star mass from  $M = 1.00 - 1.97 M_\odot$  as described in the text. In addition, we show the frequency range when varying the neutron-star radius according to the uncertainties from Ref. [64] (light-blue band) and the frequencies when correcting  $R_e$  by the suggested factor by Kobayakov and Pethick [62] (brown band). We compare with observed QPO frequencies from SGR 1806-20 (black lines) and SGR 1900+14 (purple lines).

damental crustal shear mode ( $n = 0, l = 2$ ) with free-slip boundary conditions based on our results for the inner-crust shear properties. Because we treat crust and core separately, we can parametrize the core by its mass and radius. We will vary the core mass  $M_C$  so that the total neutron-star mass ranges from  $M = 1.00 - 1.97 M_\odot$ , but we expect the mass variation to have only a small effect on the frequencies of the  $n = 0$  modes [18]. For each core mass, we choose the corresponding core radius  $R_C$  in such a way that the total neutron-star radius coincides with the mean value of the mass-radius band of Ref. [4]. This band was obtained using the same chiral interactions as used in this work and, thus, is consistent with our approach. It was constrained only by causality and the observation of  $2M_\odot$  neutron stars. To include the uncertainty in the mass-radius band, we will vary the neutron-star radii within its boundaries. Doing this, we obtain a neutron-star crust thickness of 0.64 – 1.37 km for a typical  $1.4M_\odot$  neutron star for our crust EOS, in very good agreement with the findings of Ref. [72].

We use the Newtonian perturbation model employed in Ref. [65] with the  $l$  scaling of Ref. [18], leading to the perturbation equation for toroidal shear modes,

$$\frac{(\mu\xi')'}{\rho_C} + v_A^2 \xi'' + \left( \omega^2 \left( 1 + \frac{v_A^2}{c^2} \right) - \frac{(l^2 + l - 2)\mu}{\rho_C R^2} \right) \xi = 0, \quad (23)$$

where  $\xi$  is the displacement, which has only a horizon-



tal component, primes correspond to derivatives with respect to the vertical direction,  $v_A = B/(4\pi\rho_C)^{1/2}$  is the Alfvén speed with the magnetic field  $B$ ,  $\omega = 2\pi f$  the frequency of the shear mode, and  $R$  the neutron-star radius. We choose  $B = 10^{14} - 10^{15} G$ , but for the fundamental mode the influence of the magnetic field is negligible. The first radial overtone, however, changes for field strengths above  $10^{15} G$  [58, 65, 70].

We solve the perturbation equation (23) with the following boundary conditions. At the ocean/crust interface, at densities of  $\approx 5 \cdot 10^7 \text{ g cm}^{-3}$ , we assume no horizontal shear stress or traction,  $\xi'(R) = 0$ . We then vary the frequency  $\omega$  until we find a solution with no horizontal shear stress or traction at the crust-core boundary,  $\xi'(R_C) = 0$  (because crust and core are decoupled). We finally correct the obtained frequency for gravitational redshift,

$$f_{\text{obs}} = f_{\text{emit}} \sqrt{1 - \frac{r_S}{R}}, \quad (24)$$

with the Schwarzschild radius  $r_S = 2GM/c^2$ . The obtained frequencies will depend on the crust thickness  $\Delta R$ , the neutron-star mass  $M$  and radius  $R$ .

We present our results for the fundamental crustal shear mode in Fig. 8. We show bands for all considered sources of uncertainty (each band also includes the EOS uncertainties and the mass variation), and compare with the lowest observed QPO frequencies as well as with the results of Ref. [18]. The latter range from 7 – 22 Hz and include a neutron-star mass variation from  $1.2 - 1.97 M_\odot$ . These results are only compatible with the 18 Hz QPO from SGR 1806-20. When setting  $R_e = 1$ , as in Ref. [18], we obtain frequencies of 16.2 – 23.5 Hz for a mass variation in the same range. Both calculations, thus, are in very good agreement, and consistent with the shear speeds of Fig. 7.

Considering superfluid neutrons and entrainment effects, the dynamical mass density decreases and the shear velocities increase. This also leads to an increase of the fundamental frequencies. For a higher entrainment coefficient  $R_e$  the frequencies are lower, while less entrainment leads to higher frequencies. Using the  $R_e$  values from Ref. [15], we obtain a frequency band of 18.3 – 28.1 Hz for a mass variation of  $M = 1.00 - 1.97 M_\odot$  (blue band), approximately 10% higher than for neglecting entrainment. Roughly 50% of the uncertainty stems from the mass variation, and  $\approx 50\%$  from the uncertainty in the crust EOS.

We show the dependence of the fundamental frequency on the different neutron star masses in the lower panel of Fig. 9. For the lightest neutron star we obtain a frequency range of 22.9 – 28.1 Hz, and for the heaviest neutron star we obtain a range of 18.3 – 22.6 Hz: Lower mass stars will have slightly higher shear frequencies. These frequencies are compatible with the observed 28 – 29 Hz QPOs for a neutron-star mass around  $1.0 M_\odot$ . We also show the uncertainty due to radius variation for same-mass neutron stars (light-blue band). This band reflects

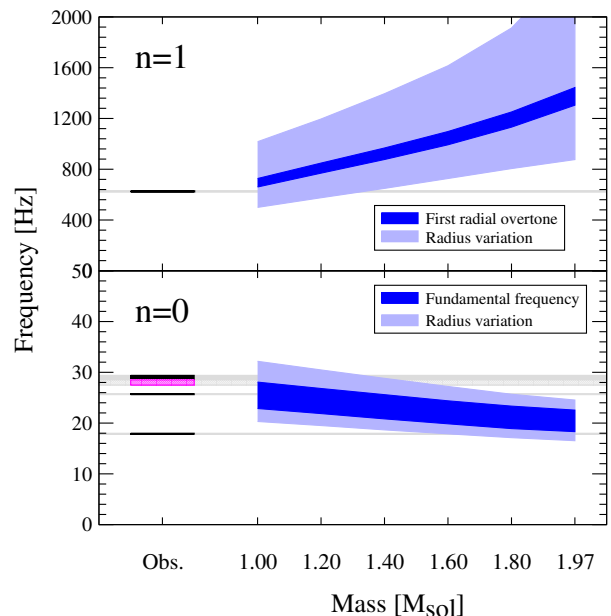


FIG. 9. Lower panel: Frequencies of the  $n = 0, l = 2$  fundamental shear mode for  $R_e$  from Ref. [15] and various neutron-star masses (blue band). We also show the uncertainties from radius variation (light-blue band), and compare to the lowest observed QPO frequencies from SGR 1806-20 (black lines) and SGR 1900+14 (purple line). Upper panel: The same for the  $n = 1$  first radial overtone compared to the observed 626 Hz QPO.

the uncertainty of the core EOS. For each individual neutron star, the uncertainties due to the crust EOS and the core EOS are of similar size. Including the radius variation, the uncertainty band for the fundamental shear mode grows to 16.5 – 32.2 Hz, see also Fig. 8. This range is compatible with the 28 Hz QPO for stars with masses  $M \leq 1.4 M_\odot$  and with the 18 Hz QPO for heavy neutron stars with  $M \geq 1.6 M_\odot$ .

Contrary to the EOS uncertainties, the uncertainties in the crust modeling affect the frequency range only modestly. Compared to our original band (without radius variation, 18.3 – 28.1 Hz), the effect due to different surface parameters is almost negligible, and the range increases to 18.0 – 28.4 Hz. The variation of the proton number of the crust nuclei,  $Z$ , increases the uncertainty range mildly to 16.3 – 29.9 Hz. This behavior is consistent with the shear velocities of Fig. 7. The variation of  $R_e$  has a sizeable impact on the results, which is already clear from the shear velocities. A variation of  $R_e$  from full to no entrainment leads to an uncertainty band of 16.2 – 42.9 Hz. Entrainment, thus, is a major source of uncertainty, in addition to the EOS uncertainty.

The blue frequency band (using  $R_e$  values of Ref. [15]) is only compatible with any observed QPO frequency for very light or very heavy neutron stars. Reference [62] suggested that lattice vibrations can reduce  $R_e$ , and, in the relevant density regime, the authors found a correction factor of  $\approx 0.4$ . Multiplying  $R_e$  by a constant correction

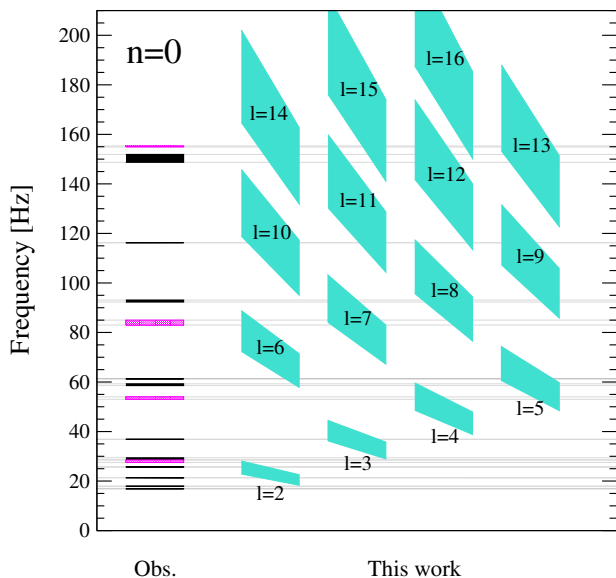


FIG. 10. Frequencies of the  $n = 0$  modes for  $2 \leq l \leq 16$  for  $R_e$  from Ref. [15]. For each  $l$ , we show the frequencies obtained for a  $1.00M_\odot$  neutron star (left boundary) up to a  $1.97M_\odot$  neutron star (right boundary). We compare with observed QPO frequencies from SGR 1806-20 (black lines) and SGR 1900+14 (purple lines).

factor of this magnitude (which is a good approximation in the density range between  $n = 0.01 - 0.06 \text{ fm}^{-3}$ ) leads to a frequency band of  $23.5 - 34.6 \text{ Hz}$ , which is in very good agreement with the observed  $28 - 29 \text{ Hz}$  QPO frequencies for all neutron-star masses. Additional effects may influence the fraction of entrained neutrons, e.g., neutron pairing, and a better understanding of neutron entrainment is a necessary condition for obtaining neutron-star properties from asteroseismology.

Combining all sources of uncertainty, we find the lowest fundamental pure crustal shear frequency, which is consistent with current nuclear-physics constraints, to be  $13.1 \text{ Hz}$ , while the highest frequency is  $52.3 \text{ Hz}$ . Current uncertainties lead to a sizeable frequency range. This range may additionally increase if nuclear pasta phases are considered. For the frequency of the fundamental mode, Ref. [17] found a reduction of up to 40% when pasta phases are included, while the effect is weaker for higher-frequency shear modes. Nevertheless, if one were to match an observed QPO frequency with the fundamental crustal shear mode, then based on our calculations an identification with the  $28 - 29 \text{ Hz}$  QPO seems to be likely.

Finally, for the simple parametrization and the same parameters chosen to obtain the blue band, we find a frequency range of  $19.6 - 26.7 \text{ Hz}$ , see Fig. 8. The two parametrizations are in excellent agreement because the fundamental mode frequency is mainly sensitive to the shear velocities at higher densities, where both parametrizations agree.

## V. HIGHER SHEAR MODES

In addition to the lowest observed QPO frequencies of  $18 - 29 \text{ Hz}$ , several other frequencies up to  $1800 \text{ Hz}$  have been observed. A large number of them, with frequencies up to  $\approx 160 \text{ Hz}$ , may be identified with higher- $l$  overtones of the fundamental  $n = 0$  mode, while the QPO at  $624 \text{ Hz}$  was identified as the first radial  $n = 1$  overtone.

In Fig. 10, we show the observed frequencies up to  $160 \text{ Hz}$  from Refs. [8, 9, 11, 12] and compare these to calculated pure crustal oscillation frequencies for  $n = 0$  and  $2 \leq l \leq 16$ . For each oscillation mode, we show the frequency variation for different masses ranging from  $1.0 - 1.97M_\odot$ , similar to Fig. 9. For every given mass, every observed frequency above  $60 \text{ Hz}$  could be matched with a certain crustal shear mode within nuclear physics uncertainties. We find gaps only between the lowest shear modes with  $l = 2, 3, 4, 5$ . At higher frequencies, due to the larger uncertainties, bands for different modes start to overlap and could be identified with the same observed QPO frequency. A possible mode assignment, thus, is ambiguous. Our results are in good agreement with the results of Ref. [17].

Nevertheless, if one were to match observed QPO frequencies with pure crustal modes and identify the  $28 - 29 \text{ Hz}$  QPO mode as the fundamental  $n = 0, l = 2$  frequency, then both sources SGR 1806-20 and SGR 1900+14 seem to be lower-mass neutron stars, with SGR 1900+14 being heavier than SGR 1806-20. The observed QPOs below  $100 \text{ Hz}$  then could be identified with  $l = 4$  and  $l = 6$  modes, while the QPO at  $37 \text{ Hz}$  does not seem to correspond to any crustal oscillation mode. The parameter  $R_e$ , though, will have a strong impact on all calculated frequencies, and a possible reduction of  $R_e$ , as suggested by Ref. [62], will move all bands up, as shown in the previous section.

We now turn to the  $n = 1$  radial overtone. In Fig. 9, we show results for the  $n = 1$  overtone for different neutron stars with masses ranging from  $1.0 - 1.97M_\odot$ . For a  $1.0M_\odot$  neutron star, we obtain a frequency range of  $660 - 727 \text{ Hz}$ , while for the  $1.97M_\odot$  neutron star we obtain a range of  $1305 - 1443 \text{ Hz}$ . The mass dependence of the first radial overtone can easily be understood because this mode strongly depends on the crust thickness. Heavier neutron stars have thinner crusts than lower-mass neutron stars and thinner crusts require higher frequencies to fulfill the boundary conditions. If the observed  $624 \text{ Hz}$  QPO is identified with the first radial overtone, this suggests that SGR 1806-20 is a lower-mass neutron star, which is consistent with our results for the  $n = 0$  shear modes.

We also show the uncertainties when varying the neutron-star radius, as before. This has a sizeable effect on the first radial overtone and lowering the radius for a  $1.0M_\odot$  neutron star can increase the frequency up to  $1017 \text{ Hz}$ . Increasing the radius can decrease the frequency to  $500 \text{ Hz}$ . This can again be understood in terms of crust thickness: For a neutron star of a given mass,

smaller (larger) radii lead to thinner (thicker) crusts. For the heaviest neutron star, we find a total frequency range of 876 – 2436 Hz when varying the radius.

These results lead to a total uncertainty band for the first radial overtone of 500 – 2436 Hz originating only in the EOS and mass uncertainty. When additionally varying  $R_e$ , the uncertainty increases to 454 – 4136 Hz. This illustrates that QPOs can in principle be a powerful tool to infer properties of neutron stars and/or constrain the EOS of nuclear matter but within current uncertainties a mode identification is not possible. Considering global oscillation modes is likely to increase the uncertainty which makes mode identification even more difficult. Additional information is needed to make robust predictions. An improved determination of  $R_e$  with small uncertainties would be a very useful first step.

## VI. SUMMARY AND OUTLOOK

In this paper we have studied the influence of different sources of uncertainty on the spectrum of shear modes in the neutron-star inner crust. To capture the uncertainties in the nuclear interactions we used parametrizations for the energy per particle of nuclear matter, which were fit to chiral EFT calculations of pure neutron matter and the empirical saturation point. Using these interactions, we modeled the inner-crust in the Wigner-Seitz approximation and studied the impact of uncertainties in the crust composition and the surface energy parameters. While the uncertainty in the crust composition has the largest impact on the geometry of the Wigner-Seitz cell, the uncertainty in the inner-crust EOS is dominated by the nuclear interactions.

Using the inner-crust model, we determined the shear modulus and shear velocities in the neutron star crust with uncertainties. For the shear modulus we found that the main uncertainty stems from the crust composition at low densities and from the neutron-matter EOS at higher densities. For the shear velocities, the main source of uncertainty is neutron entrainment, which leads to a variation up to factor of two in the neutron-star crust.

Using free-slip boundary conditions, we calculated the frequencies of the fundamental crustal shear modes and compared our calculation to observed QPO frequencies. We obtained fundamental frequencies ranging from 18 – 28 Hz, with a total uncertainty band of 13 – 52 Hz. We identified three major sources of uncertainty: First the EOS of nuclear matter up to saturation density, which sets our inner-crust EOS, second the EOS above

saturation density, which enters our calculation via the radius variation, and third, the entrainment factor. The effect of the uncertainties in the crust composition and surface parameters on the shear-mode frequencies, instead, are small. Both an improved description of the EOS with reduced theoretical uncertainties and a better determination of the entrainment factor are necessary to reliably model crustal shear oscillations. Corrections to the value of entrainment, as suggested in Ref. [62], lower the number of neutrons locked in the lattice and lead to an increase of the calculated fundamental frequencies to 24 – 35 Hz. If the fundamental QPO frequencies can be described in terms of crustal shear modes, an identification of the fundamental shear mode with the 28 – 29 Hz QPO, thus, seems to be likely.

We also performed calculations of oscillation modes with  $n = 0$  and  $2 \leq l \leq 16$  as well as of the  $n = 1, l = 2$  mode. These calculations are very dependent on the neutron-star parameters, but show that every observed QPO frequency could be described by at least one crustal shear mode within uncertainties. While QPOs in principle could be used to infer neutron-star properties, current uncertainties are quite sizeable and hinder the clear identification of modes, which, in turn, impedes the extraction of robust constraints. The computation of shear modes in the neutron-star crust would mostly benefit from a reduction of a) the uncertainty of the EOS of neutron matter at densities below and above saturation density, and b) a determination of the entrainment factor with robust theoretical uncertainties. In addition, the influence of nuclear pasta phases has to be investigated in detail. Together with a global neutron-star oscillation model, which properly includes the effects of the strong magnetic fields, these improvements would allow comparisons with observed frequencies to reliably identify modes and infer properties of neutron stars. On the other hand, additional information on the QPO sources, e.g., masses, would allow to put constraints on the EOS or the entrainment factor.

## ACKNOWLEDGMENTS

The author thanks Sanjay Reddy and Achim Schwenk for valuable input and feedback on the manuscript. We also thank Nicolas Chamel, Christian Drischler, Dmitry Kobyakov, and Anna Watts for useful discussions. This work was supported by the National Science Foundation under Grant No. PHY-1430152 (JINA Center for the Evolution of the Elements) and by the US DOE Grant No. DE-FG02-00ER41132.

---

[1] P. Demorest, T. Pennucci, S. Ransom, M. Roberts, and J. Hessels, *Nature* **467**, 1081 (2010), arXiv:1010.5788 [astro-ph.HE].

[2] J. Antoniadis, P. C. Freire, N. Wex, T. M. Tauris, R. S. Lynch, *et al.*, *Science* **340**, 6131 (2013), arXiv:1304.6875 [astro-ph.HE].

- [3] J. M. Lattimer, *Gen. Rel. Grav.* **46**, 1713 (2014).
- [4] K. Hebeler, J. M. Lattimer, C. J. Pethick, and A. Schwenk, *Astrophys. J.* **773**, 11 (2013), arXiv:1303.4662 [astro-ph.SR].
- [5] A. L. Watts *et al.*, *Rev. Mod. Phys.* **88**, 021001 (2016), arXiv:1602.01081 [astro-ph.HE].
- [6] A. S. Schneider, C. J. Horowitz, J. Hughto, and D. K. Berry, *Phys. Rev.* **C88**, 065807 (2013), arXiv:1307.1678 [nucl-th].
- [7] N. Chamel and P. Haensel, *Living Rev. Rel.* **11**, 10 (2008), arXiv:0812.3955 [astro-ph].
- [8] G. Israel, T. Belloni, L. Stella, Y. Rephaeli, D. Gruber, *et al.*, *Astrophys. J.* **628**, L53 (2005), arXiv:astro-ph/0505255 [astro-ph].
- [9] T. E. Strohmayer and A. L. Watts, *Astrophys. J.* **632**, L111 (2005), arXiv:astro-ph/0508206 [astro-ph].
- [10] A. L. Watts and T. E. Strohmayer, *Astrophys. J.* **637**, L117 (2006), arXiv:astro-ph/0512630 [astro-ph].
- [11] T. E. Strohmayer and A. L. Watts, *Astrophys. J.* **653**, 593 (2006), arXiv:astro-ph/0608463 [astro-ph].
- [12] V. Hambaryan, R. Neuhaeuser, and K. D. Kokkotas, *Astron. Astrophys.* **528**, A45 (2011), arXiv:1012.5654 [astro-ph.SR].
- [13] R. C. Duncan, *Astrophys. J.* **498**, L45 (1998), arXiv:astro-ph/9803060 [astro-ph].
- [14] N. Andersson, K. Glampedakis, and L. Samuelsson, *Mon. Not. Roy. Astron. Soc.* **396**, 894 (2009), arXiv:0812.2417 [astro-ph].
- [15] N. Chamel, *Phys. Rev.* **C85**, 035801 (2012), arXiv:1203.0119 [nucl-th].
- [16] M. Gearheart, W. G. Newton, J. Hooker, and B.-A. Li, *Mon. Not. Roy. Astron. Soc.* **418**, 2343 (2011), arXiv:1106.4875 [astro-ph.SR].
- [17] A. Passamonti and J. A. Pons, (2016), arXiv:1606.02132 [astro-ph.HE].
- [18] A. W. Steiner and A. L. Watts, *Phys. Rev. Lett.* **103**, 181101 (2009), arXiv:0902.1683 [astro-ph.HE].
- [19] G. Baym, C. Pethick, and P. Sutherland, *Astrophys. J.* **170**, 299 (1971).
- [20] S. B. Ruester, M. Hempel, and J. Schaffner-Bielich, *Phys. Rev.* **C73**, 035804 (2006), arXiv:astro-ph/0509325 [astro-ph].
- [21] E. Epelbaum, H.-W. Hammer, and U.-G. Meißner, *Rev. Mod. Phys.* **81**, 1773 (2009), arXiv:0811.1338 [nucl-th].
- [22] R. Machleidt and D. R. Entem, *Phys. Rept.* **503**, 1 (2011), arXiv:1105.2919 [nucl-th].
- [23] K. Hebeler, J. D. Holt, J. Menendez, and A. Schwenk, *Ann. Rev. Nucl. Part. Sci.* **65**, 457 (2015), arXiv:1508.06893 [nucl-th].
- [24] K. Hebeler and A. Schwenk, *Phys. Rev.* **C82**, 014314 (2010), arXiv:0911.0483 [nucl-th].
- [25] K. Hebeler, S. K. Bogner, R. J. Furnstahl, A. Nogga, and A. Schwenk, *Phys. Rev.* **C83**, 031301 (2011), arXiv:1012.3381 [nucl-th].
- [26] J. W. Holt, N. Kaiser, and W. Weise, *Phys. Rev.* **C87**, 014338 (2013), arXiv:1209.5296 [nucl-th].
- [27] I. Tews, T. Krüger, K. Hebeler, and A. Schwenk, *Phys. Rev. Lett.* **110**, 032504 (2013), arXiv:1206.0025 [nucl-th].
- [28] G. Baardsen, A. Ekström, G. Hagen, and M. Hjorth-Jensen, *Phys. Rev.* **C88**, 054312 (2013), arXiv:1306.5681 [nucl-th].
- [29] C. Drischler, V. Somà, and A. Schwenk, *Phys. Rev.* **C89**, 025806 (2014), arXiv:1310.5627 [nucl-th].
- [30] G. Hagen, T. Papenbrock, A. Ekström, K. A. Wendt, G. Baardsen, *et al.*, *Phys. Rev.* **C89**, 014319 (2014), arXiv:1311.2925 [nucl-th].
- [31] A. Roggero, A. Mukherjee, and F. Pederiva, *Phys. Rev. Lett.* **112**, 221103 (2014), arXiv:1402.1576 [nucl-th].
- [32] G. Wlazowski, J. W. Holt, S. Moroz, A. Bulgac, and K. J. Roche, *Phys. Rev. Lett.* **113**, 182503 (2014), arXiv:1403.3753 [nucl-th].
- [33] J. E. Lynn, J. Carlson, E. Epelbaum, S. Gandolfi, A. Gezerlis, *et al.*, *Phys. Rev. Lett.* **113**, 192501 (2014), arXiv:1406.2787 [nucl-th].
- [34] A. Carbone, A. Rios, and A. Polls, *Phys. Rev.* **C90**, 054322 (2014), arXiv:1408.0717 [nucl-th].
- [35] J. E. Lynn, I. Tews, J. Carlson, S. Gandolfi, A. Gezerlis, K. E. Schmidt, and A. Schwenk, *Phys. Rev. Lett.* **116**, 062501 (2016), arXiv:1509.03470 [nucl-th].
- [36] C. Drischler, K. Hebeler, and A. Schwenk, (2015), arXiv:1510.06728 [nucl-th].
- [37] T. Otsuka, T. Suzuki, J. D. Holt, A. Schwenk, and Y. Akaishi, *Phys. Rev. Lett.* **105**, 032501 (2010), arXiv:0908.2607 [nucl-th].
- [38] G. Hagen, M. Hjorth-Jensen, G. R. Jansen, R. Machleidt, and T. Papenbrock, *Phys. Rev. Lett.* **108**, 242501 (2012), arXiv:1202.2839 [nucl-th].
- [39] G. Hagen, M. Hjorth-Jensen, G. R. Jansen, R. Machleidt, and T. Papenbrock, *Phys. Rev. Lett.* **109**, 032502 (2012), arXiv:1204.3612 [nucl-th].
- [40] A. Cipollone, C. Barbieri, and P. Navrátil, *Phys. Rev. Lett.* **111**, 062501 (2013), arXiv:1303.4900 [nucl-th].
- [41] H. Hergert, S. Binder, A. Calci, J. Langhammer, and R. Roth, *Phys. Rev. Lett.* **110**, 242501 (2013), arXiv:1302.7294 [nucl-th].
- [42] J. D. Holt, J. Menendez, and A. Schwenk, *Eur. Phys. J.* **A49**, 39 (2013), arXiv:1108.2680 [nucl-th].
- [43] J. D. Holt, T. Otsuka, A. Schwenk, and T. Suzuki, *J. Phys.* **G39**, 085111 (2012), arXiv:1009.5984 [nucl-th].
- [44] F. Wienholtz, D. Beck, K. Blaum, C. Borgmann, M. Breitenfeldt, *et al.*, *Nature* **498**, 346 (2013).
- [45] H. Hergert, S. K. Bogner, T. D. Morris, S. Binder, A. Calci, J. Langhammer, and R. Roth, *Phys. Rev.* **C90**, 041302 (2014), arXiv:1408.6555 [nucl-th].
- [46] V. Somà, A. Cipollone, C. Barbieri, P. Navrátil, and T. Duguet, *Phys. Rev.* **C89**, 061301 (2014), arXiv:1312.2068 [nucl-th].
- [47] E. Epelbaum, H. Krebs, T. A. Lähde, D. Lee, U.-G. Meißner, *et al.*, *Phys. Rev. Lett.* **112**, 102501 (2014), arXiv:1312.7703 [nucl-th].
- [48] G. Hagen *et al.*, *Nature Phys.* **12**, 186 (2015), arXiv:1509.07169 [nucl-th].
- [49] R. F. Garcia Ruiz *et al.*, *Nature Phys.* **12**, 594 (2016), arXiv:1602.07906 [nucl-ex].
- [50] T. Krüger, I. Tews, B. Friman, K. Hebeler, and A. Schwenk, *Phys. Lett.* **B726**, 412 (2013), arXiv:1307.2110 [nucl-th].
- [51] S. Gandolfi, J. Carlson, and S. Reddy, *Phys. Rev.* **C85**, 032801 (2012), arXiv:1101.1921 [nucl-th].
- [52] J. M. Lattimer and M. Prakash, (2015), arXiv:1512.07820 [astro-ph.SR].
- [53] J. M. Lattimer and Y. Lim, *Astrophys. J.* **771**, 51 (2013), arXiv:1203.4286 [nucl-th].
- [54] A. W. Steiner, *Phys. Rev.* **C77**, 035805 (2008), arXiv:0711.1812 [nucl-th].
- [55] G. Audi, M. Wang, A. H. Wapstra, F. G. Kondev, M. MacCormick, and X. Xu, *Nucl. Data Sheets* **120**, 1 (2014).

- [56] F. Douchin and P. Haensel, *Astron. Astrophys.* **380**, 151 (2001), arXiv:astro-ph/0111092 [astro-ph].
- [57] J. W. Negele and D. Vautherin, *Nucl. Phys.* **A207**, 298 (1973).
- [58] A. T. Deibel, A. W. Steiner, and E. F. Brown, *Phys. Rev.* **C90**, 025802 (2014), arXiv:1303.3270 [astro-ph.HE].
- [59] D. G. Ravenhall, C. J. Pethick, and J. R. Wilson, *Phys. Rev. Lett.* **50**, 2066 (1983).
- [60] T. Strohmayer, H. M. van Horn, S. Ogata, H. Iyetomi, and S. Ichimaru, *ApJ.* **375**, 679 (1991).
- [61] R. T. Farouki and S. Hamaguchi, *Phys. Rev.* **E47**, 4330 (1993).
- [62] D. Kobyakov and C. J. Pethick, *Phys. Rev.* **C87**, 055803 (2013), arXiv:1303.1315 [nucl-th].
- [63] S. K. Lander, N. Andersson, D. Antonopoulou, and A. L. Watts, *Mon. Not. Roy. Astron. Soc.* **449**, 2047 (2015), arXiv:1412.5852 [astro-ph.HE].
- [64] K. Hebeler, J. M. Lattimer, C. J. Pethick, and A. Schwenk, *Phys. Rev. Lett.* **105**, 161102 (2010), arXiv:1007.1746 [nucl-th].
- [65] A. L. Piro, *Astrophys. J.* **634**, L153 (2005), arXiv:astro-ph/0510578 [astro-ph].
- [66] L. Samuelsson and N. Andersson, *Mon. Not. Roy. Astron. Soc.* **374**, 256 (2007), arXiv:astro-ph/0609265 [astro-ph].
- [67] Y. Levin, *Mon. Not. Roy. Astron. Soc.* **368**, L35 (2006), arXiv:astro-ph/0601020 [astro-ph].
- [68] K. Glampedakis, L. Samuelsson, and N. Andersson, *Mon. Not. Roy. Astron. Soc.* **371**, L74 (2006), arXiv:astro-ph/0605461 [astro-ph].
- [69] Y. Levin, *Mon. Not. Roy. Astron. Soc.* **377**, 159 (2007), arXiv:astro-ph/0612725 [astro-ph].
- [70] A. Colaiuda and K. D. Kokkotas, *Mon. Not. Roy. Astron. Soc.* **414**, 3014 (2011), arXiv:1012.3103 [gr-qc].
- [71] M. van Hoven and Y. Levin, *Mon. Not. Roy. Astron. Soc.* **410**, 1036 (2011), arXiv:1006.0348 [astro-ph.HE].
- [72] A. W. Steiner, S. Gandolfi, F. J. Fattoyev, and W. G. Newton, *Phys. Rev.* **C91**, 015804 (2015), arXiv:1403.7546 [nucl-th].